

Statistical analysis of undetected point sources in cosmic microwave background maps

F. Argüeso¹*, J. L. Sanz², R.B. Barreiro^{2,3}, D. Herranz², J. González-Nuevo⁴

¹ *Departamento de Matemáticas, Universidad de Oviedo, Avda. Calvo Sotelo s/n, 33007 Oviedo, Spain*

² *Instituto de Física de Cantabria (CSIC-UC), Avda. los Castros s/n, 39005 Santander, Spain*

³ *Departamento de Física Moderna, Universidad de Cantabria, Avda. los Castros, s/n, 39005 Santander, Spain*

⁴ *SISSA-I.S.A.S, via Beirut 4, I-34014 Trieste, Italy*

23 August 2018

ABSTRACT

Cosmic microwave background (CMB) temperature anisotropies follow a Gaussian statistical distribution in the standard inflationary model, but there are non-Gaussian contributions due to astrophysical foregrounds. The detection of the non-Gaussian signal due to extragalactic point sources and its distinction from the possible intrinsic non-Gaussianity is an issue of great importance in CMB analysis. The Mexican Hat Wavelet Family (MHWF), which has been proved very useful for the detection of extragalactic point sources, is applied here to the study of non-Gaussianity due to point sources in CMB maps. We carry out simulations of CMB maps with the characteristics of the forthcoming Planck mission at 70 and 100 GHz and filter them with the MHWF. By comparing the skewness and kurtosis of simulated maps with and without point sources, we are able to detect clearly the non-Gaussian signal due to point sources for flux limits as low as 0.4 Jy (70 GHz) and 0.3 Jy (100 GHz). The second and third members of the MHWF perform better in this respect than the Mexican Hat Wavelet (MHW1) and much better than the Daubechies 4 wavelet. We have also estimated the third order, K_3 , and fourth order, K_4 , cumulants produced by point sources at these Planck channels by means of a fit with the MHWF. The average relative errors with respect to the real values are below 12% for fluxes down to 0.6 Jy (70 GHz) and 0.4 Jy (100 GHz). The values of these cumulants allow us to distinguish between different source counts models. From the estimated cumulants and assuming a power law for the source number counts we are able to obtain the coefficients α and A of the differential number counts, $\alpha = 2.19 \pm 0.46$ ($\alpha = 2.26 \pm 0.19$), $A = 24.3 \pm 4.3$ ($A = 21.0 \pm 4.2$) for 70 (100) GHz, assuming a flux limit of 1 Jy. These results are consistent with the values obtained from simulations containing only point sources, which are: $\alpha = 2.32 \pm 0.06$ ($\alpha = 2.35 \pm 0.16$), $A = 22.1 \pm 1.5$ ($A = 20.0 \pm 3.7$) for 70 (100) GHz.

Key words: methods:statistical-cosmic microwave background

1 INTRODUCTION

According to the standard cosmological model, CMB temperature anisotropies are caused by the inhomogeneities in the distribution of matter and radiation present at the decoupling time. These inhomogeneities are the product of quantum fluctuations amplified in the inflationary era and follow a Gaussian statistical distribution. Therefore, the observed CMB anisotropies are a realization of a homogeneous and isotropic Gaussian random field on the sphere. Nevertheless, some degree of non-

Gaussianity can be introduced, for instance, by non standard inflation (Bartolo et al. 2004) or by topological defects (Turok and Spergel 1990; Durrer 1999). The analysis of the first and three-year Wilkinson Microwave Anisotropy Probe (WMAP) data by the WMAP team shows that CMB temperature fluctuations are consistent with a Gaussian distribution (Komatsu et al. 2003; Spergel et al. 2006) in agreement with the standard inflation paradigm. However, some studies have detected non-Gaussian features in the WMAP data, for instance in Vielva et al. (2004) and Cruz et al. (2005, 2006) a cold non-Gaussian spot of unknown origin was detected and studied by using the Spherical Mexican Hat Wavelet. Non-Gaussian signatures have

⁰ E-mail: argueso@uniovi.es

also been found by using different methods: phase correlations (Chiang et al. 2003; Coles et al. 2004), local curvature methods (Hansen et al. 2004; Cabella et al. 2005), multivariate analysis (Dineen and Coles 2005), Minkowski functionals (Park 2004; Eriksen et al. 2004) and higher criticism (Cayón et al. 2005).

On the other hand, astrophysical foregrounds contaminate the cosmological signal and also give rise to a non-Gaussian contribution. In particular, the emission due to point sources (radio and infrared galaxies are seen as point-like objects due to their very small projected angular size in comparison with the typical experimental resolutions) is clearly non-Gaussian (Komatsu and Spergel 2001; Komatsu et al. 2003; Argüeso et al. 2003; Pierpaoli 2003; Herranz et al. 2004; Barreiro et al. 2006). In the last few years, new high frequency ($\nu \geq 10$ GHz) surveys of radio sources have been carried out (Waldram et al. 2003; Ricci et al. 2004). All the recently published data on counts and on the emission properties of extragalactic radio sources have guided the development of new cosmological evolution models able to improve on previous ones (Dunlop and Peacock 1990; Toffolatti et al. 1998) in predicting number counts and source statistics at high radio frequencies (De Zotti et al. 2005). We will use this new model to carry out point source simulations.

It is very important to assess the degree of non-Gaussianity generated by point sources in order to distinguish it from the non-Gaussian signal coming from other origins. The ESA Planck satellite (Mandolesi et al. 1998; Puget et al. 1998), which will be launched in 2008, will analyze the CMB anisotropies with unprecedented accuracy and resolution and will make possible a very precise non-Gaussianity study, for which the use of wavelets can be very suitable.

The Mexican Hat Wavelet (MHW1) has been very useful in detecting point sources (Cayón et al. 2000; Vielva et al. 2001a,b) in CMB maps, by using the signal amplification going from real space to wavelet space. The Mexican Hat Wavelet Family (MHWF) was introduced by González-Nuevo et al. (2006) as an extension of the standard MHW1, which produced higher amplification (see below) and then a better performance at point source detection. These new wavelets were also used for point source detection in Planck maps in López-Caniego et al. (2006). The MHWF is a family of isotropic 2D wavelets obtained by applying the Laplacian operator iteratively to the 2D Gaussian.

The expression of these new wavelets in real space is

$$\psi_n(x) = \frac{(-1)^n}{2^n n!} \Delta^n \varphi(x) \quad (1)$$

where x is the radial coordinate and φ is the 2D Gaussian

$$\varphi(x) = \frac{e^{-x^2/2}}{2\pi} \quad (2)$$

Note that $\psi_1(x)$ is the standard MHW1, we call the other corresponding members of the family MHWn. Any member of the family can be written very easily in Fourier space as

$$\hat{\psi}_n(k) = \frac{k^{2n} e^{-\frac{k^2}{2}}}{2^n n!} \quad (3)$$

González-Nuevo et al. (2006) considered a point source convolved with a Gaussian instrumental beam of dispersion γ

$$\gamma = \frac{FWHM}{\sqrt{8 \log(2)}} \quad (4)$$

where FWHM denotes the Full Width Half Maximum of the instrumental beam.

The point source was embedded in a CMB map, including noise and all the relevant foregrounds. Then, they filtered the map with the first members of the MHWF at different scales R .

$$\Psi_n(\vec{x}; \vec{b}, R) \equiv \frac{1}{R^2} \psi_n\left(\frac{|\vec{x} - \vec{b}|}{R}\right), \quad (5)$$

The amplification, λ , is defined as the ratio between the intensity of the point source I_w and the rms deviation σ_w in the wavelet filtered image divided by this ratio in the original image filtered with a Gaussian-shaped instrumental beam.

$$\lambda = \frac{I_w/\sigma_w}{I_g/\sigma_g} \quad (6)$$

I_w can be calculated for the different members of the MHWF as

$$I_w = \frac{I_g \beta^{2n}}{(1 + \beta^2)^{n+1}} \quad (7)$$

with $\beta = R/\gamma$.

It was proved that when filtering CMB maps with the first three members of the MHWF at an optimal scale, R , the MHW2 and MHW3 produced a higher amplification than the standard MHW1 and were hence more effective at source detection. Other higher n members of the MHWF did not yield higher amplifications.

After removing the detected point sources, there could still be a remaining non-Gaussianity due to undetected point sources. It is of great interest to characterize this non-Gaussianity in order to distinguish it from the intrinsic one.

The detection of the non-Gaussian signal due to point sources poses a similar problem to that of point source detection, these new wavelets will enhance the signal (non-Gaussian) due to point sources, thus making it possible to detect this kind of non-Gaussianity more effectively. Since the skewness and kurtosis of a Gaussian distribution are zero and three respectively, any significant deviation from these values will mean the presence of a non-Gaussian signal, so that the skewness and the kurtosis of the wavelet filtered maps can be used as estimators of the non-Gaussianity due to point sources.

Filtering CMB maps with the MHWF at optimal scales amplifies point sources and can also be used to determine the third and fourth order cumulants produced by the point sources. From these cumulants, we can also determine the parameters A and α , if we assume that the differential number counts can be expressed as a power law $dn/ds = AS^{-\alpha}$. In Pierpaoli (2003) a chi-squared fit to a power law was explored considering the moments of the CMB maps. We have considered in this paper a chi-squared fit of the third order and fourth order cumulants of the wavelet filtered maps combining several scales including the optimal ones.

The plan of the paper is as follows: in §2, we calculate the cumulants of a wavelet filtered map from those of

the original map, this allows us to relate the skewness and kurtosis of the filtered maps to the amplification. In §3, we carry out realistic CMB simulations with and without point sources, considering the characteristics of the Planck experiment at 70 and 100 GHz and perform the non-Gaussianity detection by filtering with the MHWF. In §4, we obtain the third and fourth order cumulants produced by point sources by means of a fit of the cumulants of wavelet filtered CMB maps and we also determine the parameters α and A . Finally in §5, we draw the main conclusions of the paper.

2 SKEWNESS AND KURTOSIS OF A WAVELET FILTERED MAP

Skewness and kurtosis provide us with suitable tests for determining whether certain data come from a Gaussian distribution or not. The skewness, s , is defined as

$$s = \frac{\mu_3}{\sigma^3} \quad (8)$$

where μ_3 is the third central moment of the distribution and σ its rms deviation, the skewness is zero for a Gaussian distribution. The kurtosis, k , is the fourth central moment divided by the squared variance

$$k = \frac{\mu_4}{\sigma^4} \quad (9)$$

and its value is 3 in the Gaussian case. We are interested now in calculating the skewness and kurtosis due to point sources in a wavelet filtered map from these quantities in the original observed map. Then we consider a pixelized flat 2D image including CMB, Galactic foregrounds, instrumental noise and extragalactic point sources; these four components are independent and are added up to form the image; whereas the CMB is Gaussian and the noise is considered as non-uniform but Gaussian-distributed at each pixel, the other two are non-Gaussian.

Skewness and kurtosis can be obtained from the cumulants of the probability distribution function (pdf) $p(x)$. The characteristic function $\phi(u)$ is defined as the Fourier transform of the pdf

$$\phi(u) = \int p(x) e^{iux} dx \quad (10)$$

and the cumulant function is $K(u) = \log(\phi(u))$. The cumulants of order m , K_m , can be calculated as derivatives of the cumulant function

$$K_m = \frac{1}{i^m} \frac{d^m K(u)}{du^m} \Big|_{u=0} \quad (11)$$

The second order cumulant is the variance, the third order cumulant is the third central moment μ_3 and the fourth order cumulant is $\mu_4 - 3\sigma^4$. The advantage of using the cumulants is that when the different components of the data are independent the cumulant of the sum is the sum of the cumulants. So, the cumulant of any order of the sum of CMB, noise, point sources and other foregrounds is the sum of the cumulants of the components.

In a typical CMB experiment, the image is filtered with a Gaussian-shaped instrumental beam, this means that the map is convolved with a Gaussian function. This convolution changes the skewness and kurtosis of the original map. After

the convolution, the temperature of a pixel is a linear combination of the temperatures of the neighboring pixels in the unfiltered map. For point sources, which are not correlated (this is true for the frequencies, 70 and 100 GHz, considered in this work, as can be seen in González-Nuevo et al. (2005)), the cumulants of this linear combination can then be written as a linear combination of the cumulants of the original map. If we are filtering with a function $\varphi(x)$, the cumulant of order m , K_m^f , of the filtered image can be written as

$$K_m^f = K_m A_p^{m-1} \int \varphi^m(\vec{x}) d\vec{x} \quad (12)$$

where K_m is the original cumulant of order m in the pixelized image and A_p the pixel area. From this formula, we can obtain the cumulants of the Gaussian filtered image K_m^g from those of the original one.

$$K_m^g = K_m \frac{1}{m(2\pi)^{m-1}} \left(\frac{l}{\gamma} \right)^{2m-2} \quad (13)$$

where l is the pixel size and γ the beam dispersion, see eq. (4). We are going to filter now the image with the first three members of the MHWF, the whole process amounts to filtering the original image with a convolution of the Gaussian instrumental beam and the corresponding wavelets. We could then apply Eq.(12) with $\varphi(\vec{x})$ this convolution. Finally, we can relate the cumulants K_m^w of the wavelet filtered image to the same quantities K_m in the original pixelized image. We write the formula for a general cumulant and a general member of index n of the MHWF

$$K_m^w = K_m \frac{2\pi R^{2-2m} C_{mn}}{l^{2-2m} (1 + \beta^{-2})^{(n+1)m-1}} \quad (14)$$

in this formula $\beta = R/\gamma$, R is the wavelet scale (see eq. 5) and the coefficients C_{mn} are calculated as

$$C_{mn} = \int_0^\infty (\psi_n(x))^m x dx \quad (15)$$

This last expression can be easily computed for the first members of the MHWF and for $m=3,4$.

When we consider the skewness of the total wavelet filtered image (CMB+point sources+Galactic foregrounds+noise), it can be obtained as the total third order cumulant divided by σ_w^3 with σ_w the total rms deviation. The contribution of point sources to the total skewness of the wavelet filtered map is

$$\hat{s}_w = \frac{K_3^w}{\sigma_w^3} \quad (16)$$

where K_3^w is the third order cumulant (due to point sources) of the wavelet filtered map. The contribution of point sources to the total skewness of the Gaussian filtered map is

$$\hat{s}_g = \frac{K_3^g}{\sigma_g^3} \quad (17)$$

where K_3^g is the third order cumulant (due to point sources) of the Gaussian filtered map and σ_g the total rms deviation of the Gaussian filtered maps. Finally, by using Eqs. (13) and (14) and the definition of the amplification, λ , we can relate \hat{s}_w and \hat{s}_g . We obtain the following formula for the MHWI

$$\hat{s}_w = \frac{4}{9} (1 + \beta^2) \lambda^3 \hat{s}_g \quad (18)$$

for the MHW2, we obtain a similar formula

$$\hat{s}_w = \frac{22}{81}(1 + \beta^2)\lambda^3 \hat{s}_g \quad (19)$$

and finally for the MHW3

$$\hat{s}_w = \frac{1240}{6561}(1 + \beta^2)\lambda^3 \hat{s}_g \quad (20)$$

We want to point out that these contributions depend on the cubed amplification and will be higher for the wavelets with the highest amplifications, this suggests that MHW2 and MHW3 can be better at detecting non-Gaussianity due to point sources than MHW1. Besides, we will choose optimal scales when filtering with the MHWF so that the contribution to the skewness is maximum.

We can also obtain similar relations between the contribution of point sources \hat{k}_w to the kurtosis of the wavelet filtered maps and the contribution of point sources \hat{k}_g to the kurtosis of the beam filtered maps. So, we have for the MHW1

$$(\hat{k}_w - 3) = \frac{15}{32}(1 + \beta^2)\lambda^4(\hat{k}_g - 3) \quad (21)$$

for the MHW2

$$(\hat{k}_w - 3) = \frac{2547}{8192}(1 + \beta^2)\lambda^4(\hat{k}_g - 3) \quad (22)$$

and for the MHW3

$$(\hat{k}_w - 3) = \frac{61731}{262144}(1 + \beta^2)\lambda^4(\hat{k}_g - 3) \quad (23)$$

In this case, the contribution of point sources to the total kurtosis in the wavelet filtered map is proportional to λ^4 .

3 NON-GAUSSIANITY OF SIMULATED CMB MAPS

In this section, we are going to consider the study of the non-Gaussianity in realistic simulated CMB maps. We have carried out simulations of CMB flat 2D maps of 12.8×12.8 square degrees, generated with the cosmological parameters of the standard model (Spergel et al. 2003). We have then added the relevant Galactic foregrounds (free-free, synchrotron and dust emission), we have used the Planck Reference Sky, prepared by the members of the Planck Working Group 2. Galactic foregrounds have been selected from 12 different regions of the sky (at Galactic latitude $b > 30^\circ$). Each one of these 12 Galactic simulations has been used according to its representativeness as in López-Caniego et al. (2006).

In order to give the most realistic numbers of detected extragalactic point sources, we have adopted the model recently presented by De Zotti et al. (2005). This new model takes into account the new data coming from high frequency radio surveys of extragalactic sources and discusses all source populations contributing to the number counts at these frequencies. It has thus proven capable of giving a better fit than before to all the currently published source number counts and related statistics at $\nu \geq 10$ GHz coming from different surveys (Ricci et al. 2004; Waldram et al. 2003). This model also fits well the number counts obtained from the three year WMAP data (Hinshaw et al. 2006).

Since we are especially interested in applying our new method to the maps which will be provided by the *Planck*

mission in the near future, and given that we can be very confident in the input source model counts, we have considered the specific conditions of two *Planck* channels, which operate at 70 and 100 GHz.¹

We are going to consider that the noise is anisotropic. Anisotropic noise has been generated using the simulation pipeline for the Planck mission (Reinecke et al. 2006), that has been made available for the Planck community by the Planck LevelS team. The `simmission` code (van Leeuwen et al. 2002; Challinor et al. 2002) has been used to simulate the satellite dynamics during a mission flight of 14 months. The satellite will observe the microwave sky from the Lagrangian point L2, where it will be spin-stabilised by rotating at 1 *r.p.m.* The rotation axis will progress as the Earth moves around the Sun, therefore Planck will cover the full sky in half a year. The angle between its optical and rotation axes will be slightly less than 90° , thus Planck will scan the sky along circles. In order to cover the full sky, its rotation axis will make slow excursions from the Ecliptic plane with an amplitude of several degrees.

For this simulation we have assumed a cycloidal scanning strategy with a 7° slow variation in the Ecliptic collatitude of the z-axis. This scanning strategy implies that the sky will be covered inhomogeneously. As mentioned before, the sky is covered twice in a year. However, we have simulated a flight duration of 14 months (the nominal mission duration). In the additional 2 months a region that covers approximately 1/3 of the total area of the sky is observed one more time. Figure 1 shows the observation pattern, in Ecliptic coordinates, for the 70 GHz channel. The observation pattern is obtained from the satellite dynamics taking into account the position of the different detectors in the focal plane, so the observation pattern for 100 GHz is slightly different from the one in Figure 1. In both cases we can see a broad “ring” where the number of observations is higher than in the rest of the sky. This “ring” covers $\approx 1/3$ of the sky. Since the final noise level is inversely proportional to the square root of the number of observations, the regions inside that ring have lower noise levels than the rest of the sky. In order to generate anisotropic noise patches for our work we have taken two representative zones of the sky, one inside the “low noise” ring and other outside it. The noise rms per pixel is obtained from the number of observations inside the pixel and the detector noise equivalent temperature, that is specified in the Planck detector database. The final average noise rms levels per pixel (pixel size = $3'$) in thermodynamic $\Delta T/T$ units are 3.51×10^{-5} (1.35×10^{-5}) at 70 (100) GHz for the high noise zone and 2.19×10^{-5} (8.68×10^{-6}) at 70 (100) GHz for the low noise zone (inside the ring). To preserve the proportion of high to low noise regions in the sky we have simulated two high noise patches for every low noise patch.

We consider 1000 simulations of CMB plus anisotropic noise at 70 and 100 GHz, these simulations are Gaussian and will serve as comparison with the non-Gaussian ones, one

¹ The characteristics of the channels, relevant for our purposes, are: a) pixel sizes, $3'$ and $3'$ at 70 and 100 GHz, respectively; b) Full Width Half Maximum (FWHM) of the circular gaussian beams, $14'$ and $9.5'$, respectively. In all the cases, we have used the estimated instrument performance goals available at the web site: <http://astro.estec.esa.nl/Planck>.

third of the simulations correspond to the low noise zone and two thirds to the high noise zone. Then, we generate 1000 simulations including CMB, anisotropic noise, Galactic foregrounds and point sources for each of the following flux limits: 1Jy, 0.9 Jy, 0.8 Jy,....., 0.1 Jy, i.e. we remove all the sources above the given flux limit (the third order and fourth order cumulants of the different simulated components can be seen in Table 2). We filter all the simulations with the MHW1, MHW2 and MHW3 at the optimal scales (obtained by maximizing the amplification) and calculate their skewness and kurtosis.

Then, taking into account the skewness, we perform the following hypothesis test: we consider the null hypothesis, H_0 , the simulation is Gaussian, against the alternative hypothesis, H_1 , it is non-Gaussian. We set a significance level $\alpha = 0.05$, this means that we reject the null hypothesis when a simulation with point sources has a skewness higher than a value s_5 , which corresponds to that of the 95% of the Gaussian simulations. The test is one-sided to the right, since the simulations with point sources have positive skewness. We define the power of the test as $1 - \delta$, with δ the probability of accepting the null hypothesis when it is false, i.e. the power is the proportion of non-Gaussian simulations with a skewness higher than that of 95% of the Gaussian ones. The higher the power, the more efficient the method in detecting non-Gaussianity.

We perform the same test with the kurtosis, setting a kurtosis limit k_5 ; it is also one-sided to the right, since the kurtosis of point sources is higher than 3.

The power of these tests for the different flux limits are shown in Table 1, they are also plotted in Figure 2. At 70 GHz the power of the skewness test with a flux limit of 0.4 Jy is 8% (MHW1), 9% (MHW2) and 10% (MHW3). The power is higher for the kurtosis test : 11% (MHW1), 13% (MHW2) and 11% (MHW3) at 0.4 Jy. Therefore, for the MHW2 the probability that a patch with this flux limit has a kurtosis higher than that of 95% of the Gaussian simulations is 0.13. In practice, we could consider 126 patches (half sky) with the size of the simulated ones, if they are Gaussian the probability of finding more than 10 with a kurtosis higher than k_5 is 0.05, if we had point sources up to 0.4 Jy, this probability would be 0.95, (this can be calculated by using the binomial distribution with probabilities 0.05 and 0.13 in the Gaussian and non-Gaussian case, respectively). Therefore, the detection of non-Gaussianity would be possible for this flux limit.

For the 100 GHz channel, the results of the skewness test can also be seen in Table 1, for instance the power at 0.3 Jy is 8% (MHW1), 13% (MHW2) and 12% (MHW3). The power is higher for the kurtosis test: 9% (MHW1), 18% (MHW2), 22% (MHW3) at 0.3 Jy, making detection possible down to this flux. The kurtosis test allows the detection of non-Gaussianity at 100 GHz for lower fluxes than at 70 GHz.

We would like to comment that point sources could be detected in these channels, accepting a 5% of spurious detections, down to 0.47 Jy (70 GHz) and 0.25 Jy (100 GHz) (López-Caniego et al. 2006). Therefore, even if we were able to perform a perfect subtraction (or masking) of the point sources above these detection fluxes, we would still clearly detect a non-Gaussian signal due to unsubtracted point sources in the 70 GHz channel. For 100 GHz, at the flux cut of 0.2 Jy (i.e below the theoretical detec-

tion limit), the highest found power is 11% (corresponding to the kurtosis of the MHW3). Thus, it is likely that a non-Gaussian signal due to residual point sources is still present when analysing a presumably clean CMB map. These results show the importance of studying and characterising the non-Gaussianity due to residual point sources (or other foregrounds) in order to avoid its misidentification as intrinsic non-Gaussianity.

In general the MHW2 and MHW3 perform better than the MHW1, producing higher powers; the kurtosis test is more powerful than the skewness one and the tests are more powerful at 100 GHz than at 70 GHz, (see Table 1 and Figure 2).

In order to assess the influence of the Galactic foregrounds, we have also carried out 1000 simulations without point sources but including the Galactic foregrounds. The power in this case is always below 6% (see the no sources case in Table 1), confirming that these foregrounds contribute very little to the non-Gaussianity, when we filter with these wavelets at the optimal scales.

We have also performed similar tests by filtering the maps with the Daubechies 4 wavelet, this wavelet has been already used in the study of the non-Gaussianity of CMB maps (Barreiro and Hobson 2001). The power of the skewness and kurtosis tests with this wavelet is never higher than 50%, even for fluxes as high as 1 Jy and is always much lower than the power obtained with the MHWF, as can be seen in Figure 2. We have considered skewness and kurtosis of different detail coefficients (horizontal, vertical, diagonal) at different resolution levels and plotted in Figure 2 the power obtained for the detail coefficients which produce the highest power. It is clear that, whereas the members of the MHWF are adapted to the detection of point sources and the non-Gaussian signal they produce, this is not the case for the Daubechies family.

4 CHARACTERISING POINT SOURCES

4.1 Point source cumulants

In the previous section, we have performed Gaussianity tests in order to detect the non-Gaussian signal generated by point sources in CMB maps. The estimation of the level of this signal is also of great interest. Therefore, it is worthwhile calculating the third order cumulant, K_3 , and the fourth order cumulant, K_4 , produced by point sources. The problem is that we could only know directly the values of K_3 and K_4 of CMB maps including CMB, noise, point sources and other foregrounds, but not of the point source maps. A possible solution would be to filter the maps with suitable wavelets so that the main contribution to the cumulants would be that of point sources. As we have seen before, the MHWF at the optimal scales could perform well in this respect. Therefore, our idea is to filter CMB maps with the MHWF and to try to extract the parameters K_3 and K_4 . However, we should first relate the cumulants of a wavelet filtered map to the cumulants of the original map, this can be done by using eqs. (14) and (15). These equations for the MHW1, MHW2 and MHW3 give us the relation between the original cumulants due to point sources and the wavelet filtered cumulants.

Our goal is to estimate K_3 and K_4 from simulations

including CMB, noise, point sources and other foregrounds at 70 and 100 GHz. We filter these simulations with the MHW1, MHW2 and MHW3 at their optimal scales. We include two additional scales for each wavelet to improve the fit, one arcminute less than the optimal scale and one arcminute more than the optimal scale. So for each simulated map we calculate nine quantities c^i , the third order cumulants for the three scales and the three wavelets involved, where we have subtracted the average contribution of the anisotropic noise. We perform a chi-squared fit to the third order cumulant of the wavelet filtered maps $g^i K_3$, with g^i the coefficients, see eqs. (14) and (15), which relate the wavelet filtered third order cumulant with the original one K_3 . The chi-squared function can be written

$$\chi^2 = \sum_{i,j} C_{ij}^{-1} (c^i - g^i K_3)(c^j - g^j K_3) \quad (24)$$

with C_{ij} the covariance matrix of the wavelet filtered third order cumulants obtained from 1000 simulations including CMB plus noise. The simulations used are flat patches of $12.8 \times 12.8 \text{ deg}^2$ similar to the ones explained in section 3. Minimizing the chi-squared expression with respect to K_3 , we estimate the third order cumulant due to point sources of the original map. We carry out 126 simulations (half sky) including CMB, anisotropic noise, point sources up to a certain flux limit (from 0.1 Jy to 1 Jy) and other foregrounds. The third order and fourth cumulants of the different components of these simulations can be seen in Table 2. Note that in this Table, we write the cumulants after filtering the maps with the Gaussian instrumental beam, except for the noise.

We obtain the point source cumulant K_3 from each map through the chi-squared minimization. Finally, we calculate an average K_3 representative of half sky. We perform the same process for the fourth order cumulant K_4 . The chi-squared function is in this case

$$\chi^2 = \sum_{i,j} D_{ij}^{-1} (d^i - h^i K_4)(d^j - h^j K_4) \quad (25)$$

Now D_{ij} is the covariance matrix of the fourth order cumulants, d^i the fourth order cumulants of the wavelet filtered maps (subtracting the average anisotropic noise contribution) and h^i the coefficients which relate the wavelet filtered fourth order cumulants and the original ones. Minimizing with respect to K_4 , we estimate its value for each map. As before, we calculate an average value from 126 simulations (half sky). Finally, we calculate the average value of K_3 and K_4 from ten half skies and their corresponding rms deviations. We have also calculated these cumulants directly from simulations (unfiltered) of the same size, which only include point sources up to a certain flux limit to compare our previous estimations with the real values. The estimated values with the MHWF and the values obtained from the point source only simulations, K_3^{ps} and K_4^{ps} , are presented in Table 3 for different flux limits from 0.1 Jy to 1 Jy. We have also calculated the relative error of K_3 and K_4 with respect to K_3^{ps} and K_4^{ps} for each half sky. We write in Table 3 the average and the dispersion of this error obtained from ten half skies. We can see in this table that the average relative error of K_3 and K_4 with respect to K_3^{ps} and K_4^{ps} is below 12% down to 0.6 Jy (70 GHz) and 0.4 Jy (100 GHz), so that

values close to the real ones can be obtained down to low fluxes.

Finally, in Table 4, we write K_3^{ps} and K_4^{ps} calculated by carrying out point source simulations in which we use the Toffolatti source counts model (Toffolatti et al. 1998) as input for our source counts. It is clear that our estimations, K_3 and K_4 , (see Tables 3 and 4) would allow us to distinguish between the De Zotti and the Toffolatti model.

4.2 Fit of the counts to a power law

Differential number counts can be modeled as a function of the flux S by a power law

$$\frac{dn}{dS} = AS^{-\alpha} \quad (26)$$

Though the fit is not very good for all the fluxes (De Zotti et al. 2005), it can be suitable for a certain range of fluxes, for instance for fluxes from 0.1 Jy to 1 Jy. Being able to obtain the values of the parameters A , the amplitude, and α , the slope, can be very useful to distinguish between different source counts models and to predict the number counts in the corresponding flux ranges.

The third order and fourth order cumulants of the source temperature distribution in a pixelized map with pixel area A_p can be easily calculated from the differential number counts assuming that sources are Poissonian distributed. This is a good approximation for the frequencies (70 and 100 GHz) we are considering (González-Nuevo et al. 2005). In this case, the third order cumulant can be written

$$K_3 = A_p^{-2} g^3(x) \int_0^{S_{lim}} dS S^3 \frac{dn}{dS} \quad (27)$$

where S_{lim} is the flux limit and g is the conversion factor from fluxes to temperatures.

$$g(x) \equiv 2 \frac{(hc)^2}{(k_B T)^3} \frac{(\sinh(x/2))^2}{x^4} \quad (28)$$

and $x \equiv h\nu/k_B T$.

The formula for the fourth order cumulant is similar

$$K_4 = A_p^{-3} g^4(x) \int_0^{S_{lim}} dS S^4 \frac{dn}{dS}. \quad (29)$$

If we assume a power law for the differential number counts, we could obtain K_3 and K_4 just by introducing the expression $AS^{-\alpha}$ in the previous formulas

$$K_3 = \frac{Ag^3 S_{lim}^{4-\alpha}}{(4-\alpha)A_p^2} \quad (30)$$

$$K_4 = \frac{Ag^4 S_{lim}^{5-\alpha}}{(5-\alpha)A_p^3} \quad (31)$$

Then, A and α could be obtained from these equations, assuming that we know K_3 , K_4 and S_{lim} .

$$\alpha = \frac{4-5c}{1-c} \quad (32)$$

$$A = \frac{(4-\alpha)K_3 A_p^2}{g^3 S_{lim}^{(4-\alpha)}} \quad (33)$$

with

$$c = \frac{A_p K_4}{g K_3 S_{lim}} \quad (34)$$

After estimating K_3 and K_4 for the 70 and 100 GHz channels by using the fit with the MHWF (see the previous subsection), we can obtain the estimated values of the amplitude, A , and the slope, α for each half sky by applying eqs. (32), (33) and (34). If we consider ten half skies, we can give an average value and the rms deviation.

The results can be seen in Table 5, where they are compared with those obtained from the point source only simulations; in this last case we have used the values K_3^{ps} and K_4^{ps} , calculated previously from the point source maps. The results at 70 GHz for a 1 Jy flux limit are: $\alpha = 2.19 \pm 0.43$, $A = 24.3 \pm 4.3$, whereas we obtain from the point source simulations: $\alpha^{ps} = 2.32 \pm 0.06$, $A^{ps} = 22.1 \pm 1.5$. For this flux limit, the average relative error of α (A) with respect to α^{ps} (A^{ps}) is below 10% (15%). The estimation is not bad, but the rms deviation is high. We can obtain reasonable estimations down to 0.7 Jy. It is clear that small errors in the determination of the cumulants produce high errors in the amplitude and slope.

The values obtained from the fit for a flux limit of 1 Jy at 100 GHz are: $\alpha = 2.26 \pm 0.19$, $A = 21.0 \pm 4.2$, whereas from the point source simulations we estimate: $\alpha^{ps} = 2.35 \pm 0.16$, $A^{ps} = 20.0 \pm 3.7$. The average relative error of α (A) with respect to α^{ps} (A^{ps}) is below 5% (6%). We obtain reasonable values down to 0.7 Jy, with less dispersion than for the 70 GHz channel.

In Figure 3, the fit for both channels at 1 Jy is compared to the differential number counts of the De Zotti model, which was used for the simulations and with the estimation from the point source simulations. As can be seen in the plots, the fit is quite good for fluxes between 0.1 Jy and 1 Jy.

5 CONCLUSIONS

We have considered a natural generalization of the MHW1 on the plane, R^2 , based on the iterative application of the Laplacian operator to the MHW1. We have called this group of wavelets the Mexican Hat Wavelet Family (MHWF) (González-Nuevo et al. 2006; López-Caniego et al. 2006). We have applied the MHWF to the study of the non-Gaussianity produced in CMB maps by extragalactic point sources, a very important issue for the separation and analysis of different non-Gaussian components in the CMB.

We have first derived a formula, eq. (14), which relates the cumulants of 2D point source maps filtered with the MHWF with the cumulants of the original point source maps. From this formula, we have obtained several equations, eqs. (18-23), which relate the contribution of point sources to the skewness and kurtosis of wavelet (MHWF) filtered 2D CMB maps to their contribution to the skewness and kurtosis of beam filtered CMB maps.

According to these formulas, the skewness of a wavelet filtered map is proportional to λ^3 , with λ the amplification, and the kurtosis is proportional to λ^4 . This means that the higher the amplification the higher the non-Gaussian signal will be. Therefore, the MHW2 and MHW3 at their optimal scales can be very suitable filters to detect the non-Gaussian signal due to point sources, since they produce a higher amplification than the MHW1 (González-Nuevo et al. 2006; López-Caniego et al. 2006).

We have then considered Gaussian simulations of CMB plus anisotropic noise and compared them with simulations including all the relevant components: CMB, anisotropic noise, point sources and Galactic foregrounds. The simulations are 2D maps of 12.8×12.8 square degrees with the characteristics of the Planck experiment at 70 GHz and 100 GHz. We perform a Gaussianity test based on the skewness and kurtosis of the maps filtered with the MHW1, MHW2 and MHW3 at the optimal scales (those which produce the highest amplifications), we compare 1000 simulations of CMB plus noise with 1000 simulations including point sources up to different flux limits from 0.1 Jy to 1 Jy.

The power of the test is higher for the MHW2 and the MHW3 than for the standard MHW1, the kurtosis test is more powerful than the skewness test. We could detect the non-Gaussianity due to point sources down to a flux limit of 0.4 Jy (70 GHz) and 0.3 Jy (100 GHz), the powers are higher for 100 GHz than for 70 GHz. The results can be seen in Figure 2 and Table 1. We would like to point out that according to López-Caniego et al. (2006) point sources could be detected in these channels, assuming a 5% of spurious detections, down to 0.47 Jy (70 GHz) and 0.25 Jy (100 GHz). This means that, using the MHWF, we can see a non-Gaussian signal due to weak point sources, which are in the limit of detection of current source extraction techniques. Therefore, it is very important to characterise the non-Gaussianity due to unsubtracted point sources, in order to avoid its possible misidentification as intrinsic non-Gaussianity.

The influence of Galactic foregrounds is negligible, since when we consider simulations without point sources, but keeping the Galactic foregrounds, the powers go down below 6%. We have also studied the performance of the Daubechies 4 wavelet, obtaining powers below 50% even for flux limits as high as 1 Jy. The MHWF performs much better than this wavelet (see Figure 2), since it is adapted to deal with point sources.

This method could be used for all the frequencies of the Planck experiment and could also be extended to spherical CMB images, as the ones provided by the Planck experiment.

We have also tried to estimate the third order cumulant K_3 and the fourth order cumulant K_4 , produced by point sources at the 70 and 100 GHz Planck channels. We filter 12.8×12.8 square degrees CMB maps with the characteristics of the Planck experiment with the MHW1, MHW2 and MHW3 at three scales for each wavelet (including the optimal ones). The maps include CMB, anisotropic noise, point sources and other foregrounds. We calculate the third and fourth order cumulants of these wavelet filtered maps and write chi-squared functions, eqs. (24) and (25), which allow us to estimate the cumulants of the original point source maps; we have used eq. (14) to relate the cumulants of the wavelet filtered maps with those of the original maps. We have compared our estimated values with those, K_3^{ps} and K_4^{ps} , obtained directly from simulations of the same type but including only unfiltered point sources without any other component. The results can be seen in Table 3. The average error (from ten half skies) is below 12% down to a flux limit of 0.6 Jy (70 GHz) and 0.4 Jy (100 GHz). The determination of these cumulants would allow us to distinguish between different source counts models (see Tables 3 and 4).

Finally, we have also studied the fit of the differen-

tial number counts at 70 and 100 GHz to a power law $dn/dS = AS^{-\alpha}$. From the cumulants previously estimated, we calculate by using eqs. (32-34) the amplitude A and slope α of the differential number counts. The results at 70 GHz for a 1 Jy flux limit are: $\alpha = 2.19 \pm 0.43$, $A = 24.3 \pm 4.3$. When we calculate these magnitudes from the cumulants K_3^{ps} and K_4^{ps} , computed directly from the point source only simulations, we obtain $\alpha^{ps} = 2.32 \pm 0.06$, $A^{ps} = 22.1 \pm 1.5$. These are the average and rms deviation from ten half skies. For this flux limit, the average relative error of α (A) with respect to α^{ps} (A^{ps}) is below 10% (15%). The dispersion in the values obtained with the MHWF fit is high, though the average is consistent with the value obtained directly from point sources down to a flux limit of 0.7 Jy, as can be seen in Table 5.

When we consider the 100 GHz channel, the values obtained from the MHWF fit for a flux limit of 1 Jy are: $\alpha = 2.26 \pm 0.19$, $A = 21.0 \pm 4.2$, the results from the point source simulations are: $\alpha^{ps} = 2.35 \pm 0.16$, $A^{ps} = 20.0 \pm 3.7$. The fit is better for this channel than for the 70 GHz one, having a lower dispersion. For this flux limit, the average relative error of α (A) with respect to α^{ps} (A^{ps}) is below 5% (6%). The results are consistent down to a flux limit of 0.7 Jy. The detailed values of the parameters α and A can be seen in Table 5.

In Figure 3 we plot the differential source counts of the De Zotti model, the fit to a power law by using the MHWF and the fit obtained from the point source only simulations, in both cases with a 1 Jy flux limit. As we can see in this figure, both fits are consistent with the input counts in the range between 0.1 Jy and 1 Jy.

ACKNOWLEDGMENTS

We acknowledge partial financial support from the Spanish Ministry of Education (MEC) under project ESP2004-07067-C03-01. We thank G. De Zotti for having kindly provided us with the source number counts foreseen by the De Zotti et al. (2005) cosmological evolution model at the LFI frequencies. We acknowledge the use of the Planck Reference Sky, prepared by the members of the Planck Working Group 2. We also thank L. Toffolatti for useful discussions. Finally, we thank the referee, Mark Ashdown, for his useful comments and suggestions.

REFERENCES

- Argüeso, F., González-Nuevo, J., & Toffolatti, L., 2003, *ApJ*, 598, 86
- Barreiro, R. B. and Hobson, M. P., 2001, *MNRAS*, 327, 813.
- Barreiro, R. B., Martínez-González, E., Vielva, P., Hobson, M. P., 2006, *MNRAS*, 368, 226
- Bartolo, N., Komatsu, E., Matarrese, S., Riotto, A., 2004, *Phys. Rep.*, 402, 103
- Cabella, P., Liguori, M., Hansen, F. K., Marinucci, D., Matarrese, S., Moscardini, L., Vittorio, N., 2005, *MNRAS*, 358, 864.
- Cayón, L., Sanz, J. L., Barreiro, R. B., Martínez-González, E., Vielva, P., Toffolatti, L., Silk, J., Diego, J. M. & Argüeso, F. 2000, *MNRAS*, 313, 757
- Cayón, L., Jin, J., Treaster, A., 2005, *MNRAS*, 362, 826
- Challinor A. D., Mortlock D. J., van Leeuwen F., Lasenby A. N., Hobson M. P., Ashdown M. A. J., Efstathiou G. P., 2002, *MNRAS*, 331, 994
- Chiang, L.-Y., Naselsky, P. D., Verkhodanov, O.V., 2003, *ApJ*, 590, 65.
- Coles, P., Dineen, P., Earl, J., Wright, D., 2004, *MNRAS*, 350, 989.
- Cruz, M., Martínez-González, E., Vielva, P., Cayón, L., 2005, *MNRAS*, 356, 29.
- Cruz, M., Tucci, M., Martínez-González, E., Vielva, P., 2006, submitted to *MNRAS*, (astro-ph/0601427).
- De Zotti, G., Ricci, R., Mesa, D., Silva, L., Mazzotta, P., Toffolatti, L., and González-Nuevo, J. 2005 *A&A*, 431, 893
- Dineen, P., Coles, P., 2005, submitted to *MNRAS*, (astro-ph/0511802).
- Dunlop, J.S., & Peacock, J.A. 1990, *MNRAS*, 247, 19
- Durrer, R., 1999, *New Astron. Rev.*, 43, 111.
- Eriksen, H. K., Novikov, D. I., Lilje, P.B., Banday, A. J., Górski, K. M., 2004, *ApJ*, 612, 64.
- González-Nuevo, J., Toffolatti, L., & Argüeso, F. 2005, *ApJ*, 621, 1
- González-Nuevo, J., Argüeso, F., López-Caniego, M., Toffolatti, L., Sanz, J. L., Vielva, P., Herranz, D. 2006, *MNRAS*, 369, 1603
- Hansen, F. K., Cabella, P., Marinucci, D., Vittorio, N., 2004, *ApJL*, 607, L67.
- Herranz, D., Kurouglu, E. E., Toffolatti, L., 2004, *A&A*, 424, 1081
- Komatsu, E., and Spergel, D.N., 2001, *Phys. Rev. D*, 63, 063002
- Hinshaw, G. et al. 2006, submitted to *ApJ*, (astro-ph/0603451)
- Komatsu et al., 2003, *ApJs*, 148, 119
- López-Caniego, M., Herranz, D., González-Nuevo, J., Sanz, J. L., Barreiro, R. B., Vielva, P., Argüeso, F., Toffolatti, L., 2006, *MNRAS*, in press
- Mandolesi, N. et al. 1998, Proposal for the "Planck" Low Frequency Instrument (LFI), ESA Science Report D(SCI)-98(03)
- Park, C. G., 2004, *MNRAS*, 349, 313
- Pierpaoli, E., 2003, *ApJ*, 589, 58.
- Puget, J. L. et al. 1998, Proposal for the "Planck" High Frequency Instrument (HFI), ESA Science Report D(SCI)
- Reinecke M., Dolag K., Hell R., Bartelmann M., Enßlin T. A., 2006, *A&A*, 445, 373
- Ricci, R., et al. 2004, *MNRAS*, 354, 305
- Spergel, D.N., et al., 2003, *ApJS*, 148, 175
- Spergel, D.N., et al., 2006, submitted to *ApJ*, (astro-ph/0603449)
- Toffolatti, L., Argüeso Gómez, F., de Zotti, G., Mazzei, P., Franceschini, A., Danese, L. & Burigana, C. 1998, *MNRAS*, 297, 117
- Turok, N. & Spergel, D., 1990, *Phys. Rev. Letters*, 64, 2736
- van Leeuwen F., et al., 2002, *MNRAS*, 331, 975
- Vielva, P., Martínez-González, E., Cayón, L., Diego, J. M., Sanz, J. L. & Toffolatti, L. 2001, *MNRAS*, 326, 181
- Vielva, P., Barreiro, R. B., Hobson, M. P., Martínez-González, E., Lasenby, A. N., Sanz, J. L. & Toffolatti, L. 2001, *MNRAS*, 328, 1

Vielva, P., Martínez-González, E., Barreiro, R. B., Sanz, J.

L., Cayón, L., 2004, MNRAS, 609, 22

Waldram, E.M., et al., 2003, MNRAS, 342, 915

70 GHz	s(MHW1)	s(MHW2)	s(MHW3)	k(MHW1)	k(MHW2)	k(MHW3)
no sources	4	4	4	5	4	4
0.1 Jy	5	5	5	5	5	5
0.2 Jy	5	6	6	6	6	6
0.3 Jy	7	7	7	7	8	7
0.4 Jy	8	9	10	11	13	11
0.5 Jy	10	11	10	13	16	14
0.6 Jy	14	17	16	21	26	23
0.7 Jy	21	24	22	35	39	37
0.8 Jy	23	27	26	39	43	41
0.9 Jy	36	39	37	53	56	53
1 Jy	33	38	36	52	55	52

100 GHz	s(MHW1)	s(MHW2)	s(MHW3)	k(MHW1)	k(MHW2)	k(MHW3)
no sources	3	5	4	4	4	6
0.1 Jy	4	5	6	4	5	5
0.2 Jy	6	9	9	6	8	11
0.3 Jy	8	13	12	10	18	22
0.4 Jy	21	29	30	32	49	54
0.5 Jy	25	35	33	40	58	61
0.6 Jy	39	52	51	60	75	76
0.7 Jy	55	65	64	72	81	83
0.8 Jy	56	67	66	75	84	85
0.9 Jy	68	76	76	80	87	89
1 Jy	67	75	74	82	88	89

Table 1. Power (percentage) of the skewness and kurtosis tests at 70 and 100 GHz for different flux limits, for the first three members of the MHWF. In the first, second and third columns, we show the power of the skewness test for the MHW1, MHW2 and MHW3, respectively. In the fourth, fifth and sixth columns, we write the power of the kurtosis test for the MHW1, MHW2 and MHW3.

	K_3		K_4	
Freq(GHz)	70	100	70	100
noise(high)	$(0.07 \pm 5.9) \times 10^{-17}$	$(-0.1 \pm 2.1) \times 10^{-18}$	$(9.6 \pm 0.1) \times 10^{-19}$	$(6.9 \pm 0.1) \times 10^{-21}$
noise(low)	$(-0.3 \pm 1.9) \times 10^{-17}$	$(-0.1 \pm 1.1) \times 10^{-18}$	$(6.8 \pm 0.1) \times 10^{-20}$	$(1.43 \pm 0.02) \times 10^{-21}$
CMB	$(-0.4 \pm 3.2) \times 10^{-16}$	$(-0.5 \pm 3.7) \times 10^{-16}$	$(-2.5 \pm 1.8) \times 10^{-20}$	$(-2.3 \pm 1.9) \times 10^{-20}$
Gal.fore.	$(-4.5 \pm 0.6) \times 10^{-17}$	$(-4.0 \pm 0.5) \times 10^{-17}$	$(1.5 \pm 0.3) \times 10^{-21}$	$(1.4 \pm 0.3) \times 10^{-21}$
1 Jy	$(2.4 \pm 0.1) \times 10^{-16}$	$(1.8 \pm 0.1) \times 10^{-16}$	$(1.6 \pm 0.1) \times 10^{-20}$	$(1.4 \pm 0.1) \times 10^{-20}$
0.5 Jy	$(6.1 \pm 0.2) \times 10^{-17}$	$(4.9 \pm 0.2) \times 10^{-17}$	$(2.1 \pm 0.1) \times 10^{-21}$	$(2.0 \pm 0.1) \times 10^{-21}$
0.1 Jy	$(2.1 \pm 0.1) \times 10^{-18}$	$(1.60 \pm 0.04) \times 10^{-18}$	$(1.41 \pm 0.05) \times 10^{-23}$	$(1.29 \pm 0.04) \times 10^{-23}$

Table 2. Third order cumulant K_3 and fourth order cumulant K_4 of the different components of our simulations: noise (high noise zone), noise (low noise zone), CMB, Galactic foregrounds and point sources, up to flux limits of 1 Jy, 0.5 Jy and 0.1 Jy. The cumulants are obtained from the simulations filtered with the Gaussian beam, except for the noise. We show the average and rms deviation from ten half skies.

70 GHz	K_3	K_3^{ps}	ΔK_3	K_4	K_4^{ps}	ΔK_4
1 Jy	$(4.60 \pm 0.59) \times 10^{-13}$	$(4.45 \pm 0.20) \times 10^{-13}$	9.5 ± 4.9	$(1.02 \pm 0.12) \times 10^{-15}$	$(0.97 \pm 0.05) \times 10^{-15}$	7.4 ± 6.9
0.9 Jy	$(4.29 \pm 0.38) \times 10^{-13}$	$(4.16 \pm 0.26) \times 10^{-13}$	5.4 ± 4.4	$(9.02 \pm 1.07) \times 10^{-16}$	$(8.86 \pm 0.70) \times 10^{-16}$	6.7 ± 3.4
0.8 Jy	$(3.50 \pm 0.27) \times 10^{-13}$	$(3.45 \pm 0.22) \times 10^{-13}$	6.1 ± 5.5	$(6.76 \pm 0.72) \times 10^{-16}$	$(6.63 \pm 0.54) \times 10^{-16}$	6.2 ± 4.7
0.7 Jy	$(2.68 \pm 0.31) \times 10^{-13}$	$(2.67 \pm 0.16) \times 10^{-13}$	9.8 ± 4.9	$(4.22 \pm 0.35) \times 10^{-16}$	$(4.44 \pm 0.32) \times 10^{-16}$	5.8 ± 4.9
0.6 Jy	$(1.73 \pm 0.26) \times 10^{-13}$	$(1.73 \pm 0.05) \times 10^{-13}$	11.5 ± 10.4	$(2.38 \pm 0.26) \times 10^{-16}$	$(2.37 \pm 0.07) \times 10^{-16}$	7.8 ± 5.8
0.5 Jy	$(1.13 \pm 0.24) \times 10^{-13}$	$(1.12 \pm 0.04) \times 10^{-13}$	18.0 ± 10.0	$(1.14 \pm 0.42) \times 10^{-16}$	$(1.24 \pm 0.06) \times 10^{-16}$	26.0 ± 23.1
0.4 Jy	$(8.37 \pm 2.85) \times 10^{-14}$	$(8.80 \pm 0.42) \times 10^{-14}$	25.2 ± 18.1	$(9.54 \pm 3.03) \times 10^{-17}$	$(8.56 \pm 0.56) \times 10^{-17}$	26.7 ± 23.2
0.3 Jy	$(6.44 \pm 2.24) \times 10^{-14}$	$(4.33 \pm 0.19) \times 10^{-14}$	58.4 ± 46.7	$(4.26 \pm 2.58) \times 10^{-17}$	$(3.03 \pm 0.16) \times 10^{-17}$	77.6 ± 61.7
0.2 Jy	$(1.74 \pm 3.15) \times 10^{-14}$	$(2.08 \pm 0.08) \times 10^{-14}$	120 ± 86	$(9.89 \pm 17.71) \times 10^{-18}$	$(1.02 \pm 0.05) \times 10^{-17}$	134 ± 110
0.1 Jy	$(1.09 \pm 3.11) \times 10^{-14}$	$(3.90 \pm 0.10) \times 10^{-15}$	586 ± 538	$(7.90 \pm 34.6) \times 10^{-18}$	$(8.56 \pm 0.29) \times 10^{-19}$	3350 ± 2037
100 GHz	K_3	K_3^{ps}	ΔK_3	K_4	K_4^{ps}	ΔK_4
1 Jy	$(6.90 \pm 0.54) \times 10^{-14}$	$(6.98 \pm 0.40) \times 10^{-14}$	2.3 ± 1.7	$(8.45 \pm 0.76) \times 10^{-17}$	$(8.38 \pm 0.60) \times 10^{-17}$	2.5 ± 2.3
0.9 Jy	$(6.39 \pm 0.50) \times 10^{-14}$	$(6.54 \pm 0.41) \times 10^{-14}$	2.8 ± 2.4	$(7.42 \pm 0.69) \times 10^{-17}$	$(7.50 \pm 0.64) \times 10^{-17}$	2.5 ± 1.6
0.8 Jy	$(5.38 \pm 0.59) \times 10^{-14}$	$(5.50 \pm 0.42) \times 10^{-14}$	4.6 ± 3.2	$(5.90 \pm 0.65) \times 10^{-17}$	$(5.83 \pm 0.58) \times 10^{-17}$	3.6 ± 2.3
0.7 Jy	$(4.29 \pm 0.32) \times 10^{-14}$	$(4.25 \pm 0.24) \times 10^{-14}$	4.3 ± 2.7	$(3.86 \pm 0.29) \times 10^{-17}$	$(3.88 \pm 0.29) \times 10^{-17}$	1.9 ± 1.5
0.6 Jy	$(2.80 \pm 0.14) \times 10^{-14}$	$(2.99 \pm 0.17) \times 10^{-14}$	6.0 ± 5.3	$(2.36 \pm 0.16) \times 10^{-17}$	$(2.31 \pm 0.17) \times 10^{-17}$	4.6 ± 3.4
0.5 Jy	$(1.75 \pm 0.13) \times 10^{-14}$	$(1.88 \pm 0.09) \times 10^{-14}$	7.2 ± 7.8	$(1.23 \pm 0.07) \times 10^{-17}$	$(1.17 \pm 0.07) \times 10^{-17}$	6.1 ± 3.8
0.4 Jy	$(1.31 \pm 0.20) \times 10^{-14}$	$(1.43 \pm 0.10) \times 10^{-14}$	11.3 ± 7.4	$(7.97 \pm 0.41) \times 10^{-18}$	$(7.79 \pm 0.59) \times 10^{-18}$	4.0 ± 2.7
0.3 Jy	$(6.17 \pm 1.17) \times 10^{-15}$	$(7.19 \pm 0.27) \times 10^{-15}$	16.6 ± 14.9	$(3.35 \pm 0.39) \times 10^{-18}$	$(2.81 \pm 0.13) \times 10^{-18}$	22.8 ± 11.1
0.2 Jy	$(1.97 \pm 1.96) \times 10^{-15}$	$(3.39 \pm 0.09) \times 10^{-15}$	57.2 ± 40.4	$(1.52 \pm 0.25) \times 10^{-18}$	$(0.93 \pm 0.03) \times 10^{-18}$	63.4 ± 27.2
0.1 Jy	$(-8.30 \pm 15.4) \times 10^{-16}$	$(6.10 \pm 0.16) \times 10^{-16}$	282 ± 187	$(5.43 \pm 3.85) \times 10^{-19}$	$(7.57 \pm 0.26) \times 10^{-20}$	622 ± 476

Table 3. First and fourth columns: third order cumulant K_3 and fourth order cumulant K_4 estimated from the CMB maps by carrying out a fit with the MHWF, the average from ten half skies and the rms deviation are written. Second and fifth columns: third order cumulant K_3^{ps} and fourth order cumulant K_4^{ps} estimated from the the point source simulations (average and rms deviation from ten half skies). Third and sixth columns: relative error (percentage) of K_3 and K_4 with respect to K_3^{ps} and K_4^{ps} (average and rms deviation from ten half skies).

70 GHz	K_3^{ps}	K_4^{ps}
1 Jy	$(8.6 \pm 0.4) \times 10^{-13}$	$(1.8 \pm 0.1) \times 10^{-15}$
0.9 Jy	$(8.1 \pm 0.3) \times 10^{-13}$	$(1.6 \pm 0.1) \times 10^{-15}$
0.8 Jy	$(7.1 \pm 0.2) \times 10^{-13}$	$(1.32 \pm 0.06) \times 10^{-15}$
0.7 Jy	$(5.4 \pm 0.2) \times 10^{-13}$	$(8.7 \pm 0.5) \times 10^{-16}$
0.6 Jy	$(3.9 \pm 0.1) \times 10^{-13}$	$(5.2 \pm 0.2) \times 10^{-16}$
0.5 Jy	$(2.60 \pm 0.06) \times 10^{-13}$	$(2.8 \pm 0.1) \times 10^{-16}$
0.4 Jy	$(2.02 \pm 0.05) \times 10^{-13}$	$(1.90 \pm 0.07) \times 10^{-16}$
0.3 Jy	$(1.07 \pm 0.02) \times 10^{-13}$	$(7.3 \pm 0.2) \times 10^{-17}$
0.2 Jy	$(5.4 \pm 0.1) \times 10^{-14}$	$(2.59 \pm 0.06) \times 10^{-17}$
0.1 Jy	$(1.17 \pm 0.01) \times 10^{-14}$	$(2.55 \pm 0.03) \times 10^{-18}$
100 GHz	K_3^{ps}	K_4^{ps}
1 Jy	$(1.49 \pm 0.07) \times 10^{-13}$	$(1.7 \pm 0.1) \times 10^{-16}$
0.9 Jy	$(1.4 \pm 0.1) \times 10^{-13}$	$(1.6 \pm 0.1) \times 10^{-16}$
0.8 Jy	$(1.20 \pm 0.04) \times 10^{-13}$	$(1.24 \pm 0.06) \times 10^{-16}$
0.7 Jy	$(9.1 \pm 0.3) \times 10^{-14}$	$(8.1 \pm 0.4) \times 10^{-17}$
0.6 Jy	$(6.6 \pm 0.2) \times 10^{-14}$	$(5.0 \pm 0.2) \times 10^{-17}$
0.5 Jy	$(4.3 \pm 0.1) \times 10^{-14}$	$(2.6 \pm 0.1) \times 10^{-17}$
0.4 Jy	$(3.4 \pm 0.1) \times 10^{-14}$	$(1.81 \pm 0.05) \times 10^{-17}$
0.3 Jy	$(1.81 \pm 0.03) \times 10^{-14}$	$(6.8 \pm 0.1) \times 10^{-18}$
0.2 Jy	$(9.3 \pm 0.1) \times 10^{-15}$	$(2.46 \pm 0.04) \times 10^{-18}$
0.1 Jy	$(1.98 \pm 0.02) \times 10^{-15}$	$(2.41 \pm 0.03) \times 10^{-19}$

Table 4. Third order cumulant K_3^{ps} and fourth order cumulant K_4^{ps} calculated from the the point source simulations carried out with the source number counts of the Toffolatti et al. model (average and rms deviation from ten half skies).

70 GHz	α	α^{ps}	$\Delta\alpha$	A	A^{ps}	ΔA
1 Jy	2.19 \pm 0.43	2.32 \pm 0.06	9.9 \pm 16.1	24.3 \pm 4.3	22.1 \pm 1.5	14.9 \pm 14.9
0.9 Jy	2.08 \pm 0.50	2.10 \pm 0.12	15.5 \pm 13.4	28.3 \pm 9.4	27.0 \pm 3.6	18.9 \pm 17.2
0.8 Jy	1.81 \pm 0.72	2.03 \pm 0.12	27.2 \pm 21.1	28.3 \pm 9.4	27.0 \pm 3.6	44.6 \pm 43.3
0.7 Jy	2.24 \pm 0.46	2.06 \pm 0.05	18.6 \pm 12.3	25.2 \pm 9.4	28.8 \pm 2.6	26.5 \pm 15
100 GHz	α	α^{ps}	$\Delta\alpha$	A	A^{ps}	ΔA
1 Jy	2.26 \pm 0.19	2.35 \pm 0.16	4.2 \pm 3.5	21.0 \pm 4.2	20.0 \pm 3.7	5.6 \pm 5.9
0.9 Jy	2.16 \pm 0.14	2.23 \pm 0.13	4.3 \pm 3.8	23.4 \pm 3.4	22.9 \pm 3.2	5.7 \pm 4.9
0.8 Jy	1.84 \pm 0.26	2.07 \pm 0.12	10.9 \pm 13.7	30.6 \pm 5.7	26.5 \pm 4.1	17.5 \pm 22.1
0.7 Jy	1.93 \pm 0.16	2.14 \pm 0.11	10.0 \pm 6.6	28.6 \pm 3.7	24.8 \pm 3.8	16.4 \pm 12.6

Table 5. First and fourth columns: slope α and amplitude A of the differential number counts estimated from the CMB maps by carrying out a fit with the MHWF. Second and fifth columns: slope α^{ps} and amplitude A^{ps} estimated from the point source simulations. Third and sixth columns: relative error (percentage) of α and A with respect to α^{ps} and A^{ps} . In all the cases, we write the average and rms deviation from ten half skies

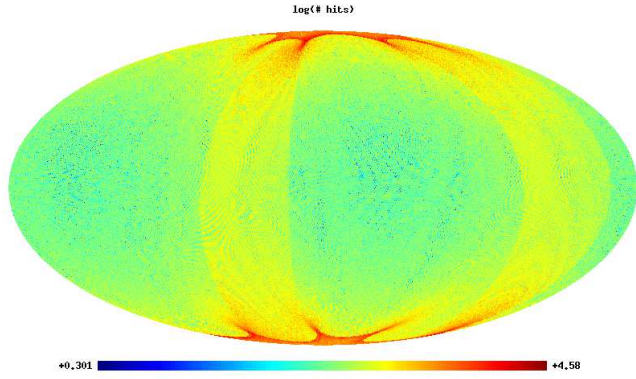


Figure 1. Observation pattern for the 70 GHz channel. The map shows the logarithm of the number of hits (number of times the detector observes a given pixel during the flight) in Ecliptic co-ordinates.

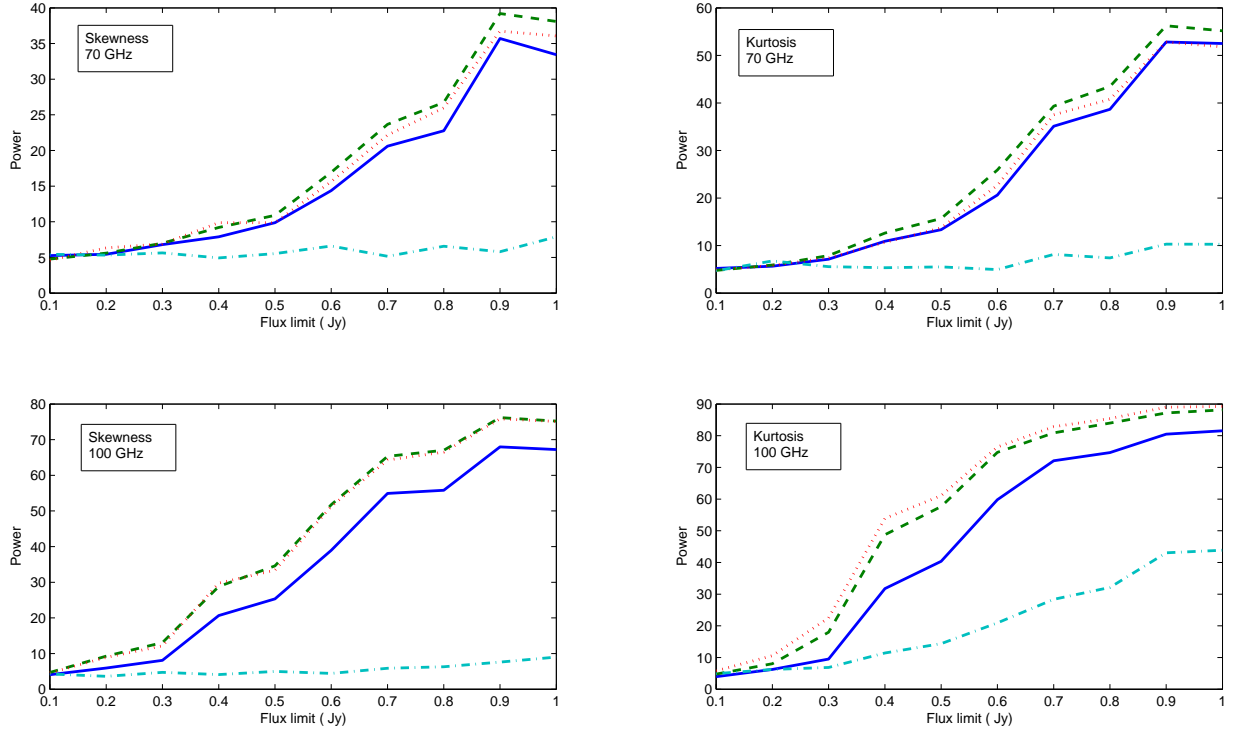


Figure 2. Power against the flux limit for the skewness test at 70 GHz (top left panel), the kurtosis test at 70 GHz (top right panel), the skewness test at 100 GHz (bottom left panel) and the kurtosis test at 100 GHz (bottom right panel). The solid line represents the MHW1 results, the dashed line the MHW2 results, the dotted line the MHW3 results and the dash-dotted line the Daubechies4 results.

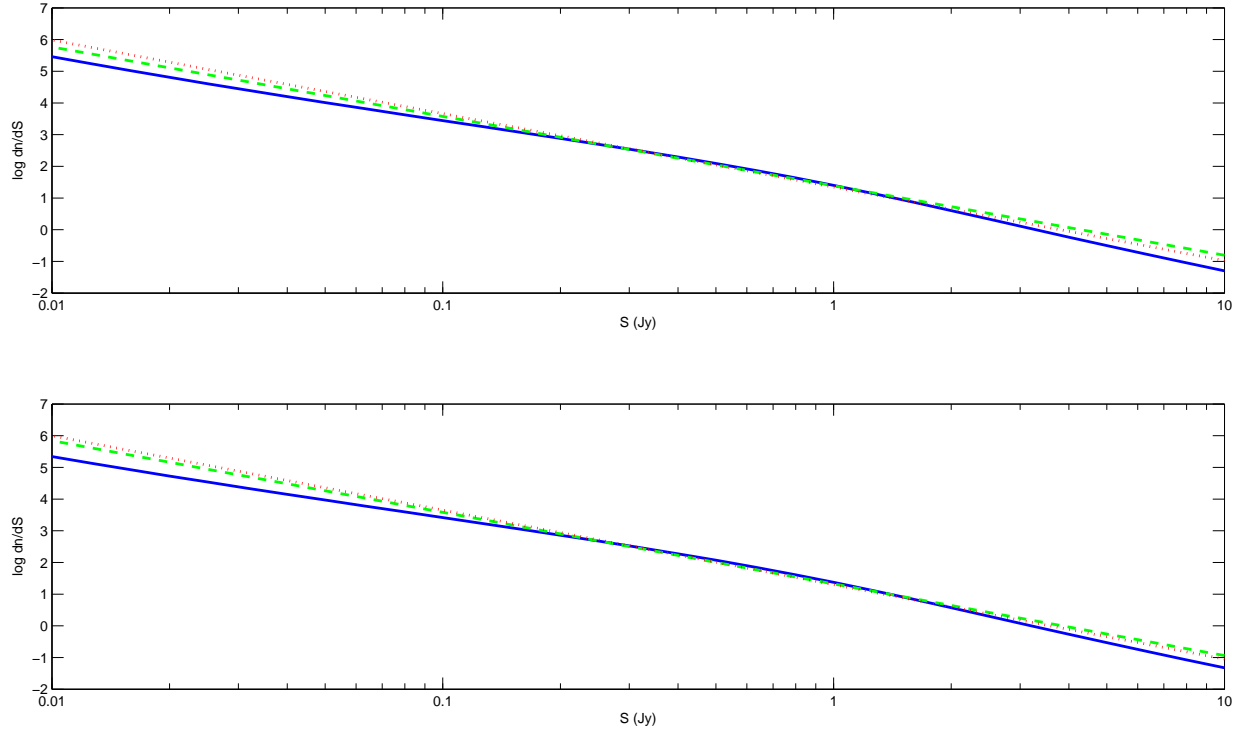


Figure 3. Top panel: (70 GHz channel) differential number counts against the flux in Jy according to the De Zotti model (solid line), the fit to a power law by using the MHWF (dashed line) with the average value of the parameters for a flux limit of 1 Jy and the same fit by using the original point source maps (dotted line) with the average value of the parameters for a flux limit of 1 Jy. Bottom panel: the same for the 100 GHz channel.